UDC 621.3 https://doi.org/10.20998/2074-272X.2025.6.05

N. Hamdi, F. Babaa, A. Touil, N. Merabet

Robust fault-tolerant sliding mode control and advanced fault diagnosis for doubly-fed induction generators

Introduction. *Doubly-fed induction generators (DFIGs) have become the preferred technology in modern wind energy systems due to their high efficiency and flexible variable-speed operation capabilities.* ***Problem.*** *Despite their advantages, DFIGs face significant challenges related to grid-connected power converters, which are susceptible to operational instability caused by voltage imbalances and electrical faults.* ***Goal.*** *This study aims to develop and validate a novel Active Fault-Tolerant Sliding Mode Control (AFT-SMC) strategy that integrates real-time fault diagnosis to enhance the reliability and stability of DFIG systems during grid disturbances. Unlike existing approaches, this work specifically addresses the reduction of false fault detections during transient events and improves fault characterization through spectral analysis.* ***Methodology.*** *The proposed control framework combines a robust sliding mode controller with a model-based fault detection and isolation system that employs adaptive thresholds and diagnostic residuals for accurate fault identification. The approach has been thoroughly tested through high-fidelity simulations under severe voltage unbalance scenarios.* ***Results.*** *Simulation outcomes demonstrate the superior performance of the proposed strategy in maintaining system stability under a 30 % voltage unbalance scenario. Specifically, the controller achieves a voltage recovery time of 0.28 s, compared to 0.42 s with conventional vector control, and reduces electromagnetic torque oscillations by approximately 45 %. Furthermore, the integrated spectral diagnosis method reaches a fault classification accuracy of 94.6 %, confirming its effectiveness in enabling early and reliable fault detection. These results validate the advantages of the proposed AFT-SMC framework in both dynamic response and fault resilience.* ***Scientific novelty.*** *The key innovation lies in the integration of a self-correcting «detect-and-adapt» mechanism that mitigates false triggers during transient grid conditions, alongside a novel spectral decomposition method for precise detection and characterization of voltage imbalances through negative-sequence component analysis.* ***Practical value.*** *This strategy significantly reduces operational costs at pilot wind farms and sets a new benchmark for intelligent fault management in renewable energy systems, with broad applicability to other power electronic interfaces in smart grids.* References 35, figures 12.

Key words: **sliding mode control, doubly-fed induction generator, active fault tolerance control, renewable energy.**

Вступ. *Асинхронні генератори з подвійним живленням (DFIGs) стали поширеними технічними рішеннями в сучасних вітроенергетичних системах завдяки своїй високій ефективності та гнучкій роботі з регульованою швидкістю.* ***Проблема***. *Незважаючи на свої переваги, DFIGs стикаються зі значними проблемами, пов'язаними з перетворювачами потужності, підключеними до мережі, які схильні до нестабільної роботи, спричиненої дисбалансом напруги та електричними несправностями.* ***Мета***. *Дане дослідження спрямоване на розробку та перевірку нової стратегії активного відмовостійкого керування ковзним режимом (AFT-SMC), яка поєднує діагностику несправностей у реальному часі для підвищення надійності та стійкості систем DFIG при порушеннях у мережі. На відміну від існуючих підходів, дана робота спрямована на зниження помилкових виявлень несправностей під час перехідних процесів та покращення характеристики несправностей за допомогою спектрального аналізу.* ***Методологія***. *Пропонована структура управління поєднує в собі надійний контролер ковзного режиму з системою виявлення та виділення несправностей на основі моделі, яка використовує адаптивні граничні значення та діагностичні залишки для точної ідентифікації несправностей. Даний підхід ретельно протестували за допомогою високоточного моделювання в умовах сильного дисбалансу напруги.* ***Результати*** *моделювання демонструють високу ефективність пропонованої стратегії підтримки стійкості системи в умовах 30 % несиметрії напруги. Зокрема, контролер досягає часу відновлення напруги 0,28 в порівнянні з 0,42 с при традиційному векторному управлінні і знижує коливання електромагнітного моменту приблизно на 45 %. Більш того, інтегрований метод спектральної діагностики досягає точності класифікації несправностей 94,6 %, що підтверджує його ефективність у забезпеченні раннього та надійного виявлення несправностей. Ці результати підтверджують переваги запропонованої структури AFT-SMC як з точки зору динамічного реагування, так і стійкості до несправностей.* ***Наукова новизна***. *Ключове нововведення полягає в інтеграції механізму «виявлення та адаптації», що самокоректується, який знижує кількість помилкових спрацьовувань в перехідних режимах мережі, а також нового методу спектрального розкладання для точного виявлення і характеристики несиметрії напруги за допомогою аналізу компонентів зворотної послідовності.* ***Практична цінність***. *Ця стратегія значно знижує експлуатаційні витрати на пілотних вітряних електростанціях та встановлює новий стандарт інтелектуального управління несправностями у системах відновлюваної енергії з широкою застосовністю до інших інтерфейсів силової електроніки в інтелектуальних мережах.* Бібл. 35, рис. 12.

Ключові слова: **ковзне управління, асинхронний генератор з подвійним живленням, активне управління відмовостійкістю, відновлювані джерела енергії.**

Introduction. Electricity plays a pivotal role in modern industrial activity, underpinning the production, transformation, and distribution of goods and services. Reliable and continuous access to electrical power is essential for maintaining industrial competitiveness, enabling efficient management of manufacturing processes, research and development, and logistics operations. In this context, the integration of renewable energy sources has gained increasing importance worldwide as a strategic approach to reducing carbon emissions and enhancing energy security [1, 2].

Among renewable technologies, wind energy stands out as a sustainable and clean alternative to fossil fuels. The efficiency of wind power generation relies heavily on the performance of electrical machines that convert the kinetic energy of the wind into electrical energy suitable for grid integration. The doubly-fed induction generator (DFIG) is the most widely used electrical machine in modern wind turbines, owing to its capability for variable-speed operation and flexible control of active and reactive power. This adaptability allows for optimal energy extraction under varying wind conditions while maintaining grid compliance [3, 4].

Despite these advantages, DFIGs are vulnerable to several operational stresses, including thermal, mechanical, electrical, and environmental factors, which can degrade their performance and reliability over time. Among electrical disturbances, voltage imbalances in the grid constitute a critical challenge. Voltage unbalance, defined as the inequality of phase voltages in a three-phase system, adversely affects the operation of DFIGs by

inducing unbalanced rotor currents. This leads to uneven electromagnetic torque, increased mechanical stress, elevated losses, and ultimately, reduced efficiency and shortened machine lifetime [5–10].

Traditional control strategies for DFIGs often lack sufficient robustness to maintain performance and stability under such unbalanced voltage conditions. Unbalanced supply voltages also negatively impact the accuracy of control algorithms, resulting in degraded power quality and potential instability in grid synchronization.

Sliding mode control (SMC) has emerged as a promising solution due to its inherent robustness against parameter variations, external disturbances, and model uncertainties [11–18]. SMC ensures precise regulation of both active and reactive power in DFIGs, providing stable operation even under fluctuating wind conditions and grid disturbances [19–26]. However, conventional SMC approaches may not adequately address the detection and mitigation of faults, especially under transient operating conditions where false fault detections are common.

To overcome these limitations, fault-tolerant sliding mode control (FT-SMC) integrates the robustness of SMC with real-time fault detection, isolation, and adaptation mechanisms. FT-SMC strategies enable the control system to maintain desired performance and stability despite the presence of faults, which is particularly critical for safety-sensitive and continuously operating systems such as wind turbines [27–32].

While various FT-SMC methods have been proposed in the literature, most treat fault detection and control adaptation separately or do not fully exploit advanced signal processing techniques for fault characterization [18]. Moreover, false alarms during transient events remain a significant practical challenge, potentially leading to unnecessary system interventions and downtime.

In light of the growing need for robust and intelligent control solutions for wind energy systems, the main objective of this study is to develop and validate a novel active fault-tolerant sliding mode control (AFT-SMC) framework for doubly-fed induction generators (DFIGs). The proposed approach aims to improve system stability and operational reliability under grid disturbances, particularly voltage unbalances, while minimizing false fault detections that often arise during transient events.

To address these challenges, the control framework combines the inherent robustness of SMC with a model-based fault detection and isolation mechanism. This fault detection and isolation system leverages adaptive thresholds and residual analysis to identify faults in real time, while a self-correcting «detect-and-adapt» logic dynamically adjusts the control response to reduce false triggers. Additionally, advanced spectral analysis is integrated into the diagnostic process through frequency-domain decomposition of stator current and instantaneous active power signals. This enables precise detection and characterization of voltage unbalance faults based on negative-sequence harmonic components.

By unifying fault-tolerant control and real-time spectral diagnosis in a single cohesive strategy, this work contributes an innovative solution that enhances both dynamic response and diagnostic accuracy for DFIG-based wind turbines operating under severe grid conditions.

DFIG mathematical model. In this study, the stator is directly linked to the grid, simplifying the system design by removing the necessity for an additional stator-side converter. This setup facilitates efficient power transfer between the DFIG and the grid while reducing energy losses. The rotor is managed via an inverter, enabling precise control of rotor speed and power flow between the rotor and the grid. This configuration allows the DFIG to operate across a broad speed range, with the capability to inject or absorb reactive power as required. The rotor speed is constrained to ±50 % of the rated speed, ensuring the system remains within practical operational limits. This limitation reduces system complexity by avoiding the need for overly intricate control mechanisms or costly components.

To streamline the dynamic analysis and control of the DFIG, the Ku transformation is employed. This transformation simplifies the system dynamics by reformulating the equations into a more tractable form using forward (f) and backward (b) reference frames. This dual-reference framework effectively decouples the control of active and reactive power in the rotor-side converter, improving the separation between mechanical and electrical dynamics. The Ku transformation optimizes control complexity without compromising system performance across diverse operating conditions, making it an essential tool for DFIG modelling, control, and simulation.

The machine equation system after Ku transformation is:

$$\begin{cases} V_{sf} = R_s i_{sf} + L_s \dfrac{\mathrm{d}i_{sf}}{\mathrm{d}t} + M \dfrac{\mathrm{d}i_{rf}}{\mathrm{d}t} + j \dfrac{\mathrm{d}\theta_s}{\mathrm{d}t} \varphi_{sf}; \\ V_{sb} = R_s i_{sb} + L_s \dfrac{\mathrm{d}i_{sb}}{\mathrm{d}t} + M \dfrac{\mathrm{d}i_{rb}}{\mathrm{d}t} - j \dfrac{\mathrm{d}\theta_s}{\mathrm{d}t} \varphi_{sb}; \\ V_{rf} = R_r i_{rf} + L_r \dfrac{\mathrm{d}i_{rf}}{\mathrm{d}t} + M \dfrac{\mathrm{d}i_{sf}}{\mathrm{d}t} + j \dfrac{\mathrm{d}\theta_r}{\mathrm{d}t} \varphi_{rf}; \\ V_{rb} = R_r i_{rb} + L_r \dfrac{\mathrm{d}i_{rb}}{\mathrm{d}t} + M \dfrac{\mathrm{d}i_{sb}}{\mathrm{d}t} - j \dfrac{\mathrm{d}\theta_r}{\mathrm{d}t} \varphi_{rb}, \end{cases} \quad (1)$$

where V_{sf}, V_{sb}, V_{rf}, V_{rb} are the *f*- and *b*-axis components of the stator and rotor voltages; i_{sf}, i_{sb}, i_{rf}, i_{rb} are the *f*- and *b*-axis components of the stator and rotor currents; R_s R_r are the stator and rotor phase resistances; L_s, L_r are the stator and rotor phase inductances; M is the mutual inductance between the stator and rotor; p is the number of pole pairs; φ_{sf}, φ_{sb}, φ_{rf}, φ_{rb} are the *f*- and *b*-axis components of the stator and rotor fluxes.

The stator and rotor flux linkages are:

$$\left[\phi_{sofb}\right] = \begin{pmatrix} L_{so} & 0 & 0 \\ 0 & L_s & 0 \\ 0 & 0 & L_s \end{pmatrix} \left[i_{sofb}\right] + \begin{pmatrix} 0 & 0 & 0 \\ 0 & M & 0 \\ 0 & 0 & M \end{pmatrix} \left[i_{rofb}\right]; \quad (2)$$

$$\left[\phi_{rofb}\right] = \begin{pmatrix} L_{ro} & 0 & 0 \\ 0 & L_r & 0 \\ 0 & 0 & L_r \end{pmatrix} \left[i_{rofb}\right] + \begin{pmatrix} 0 & 0 & 0 \\ 0 & M & 0 \\ 0 & 0 & M \end{pmatrix} \left[i_{sofb}\right], \quad (3)$$

where L_{so}, L_{ro} are the homopolar stator and rotor phase inductances; the subscripts «*rofb*» and «*sofb*» are the abbreviations in which *s*, *r* denote the stator and the rotor; *o* refers to the homopolar component; *f*, *b* indicate the forward and backward components.

The use of the Ku transformation in the electromagnetic torque results in:

$$T_e = p \cdot M \cdot \left[i_{sb} \cdot i_{rf} - i_{sf} \cdot i_{rb}\right]. \quad (4)$$

The active and reactive powers of the stator and rotor are incorporated into the control framework following the application of the Ku transformation:

$$\begin{cases} P_s = 2 \cdot V_{sf} \cdot i_{sf}; \\ Q_s = 2 \cdot V_{sf} \cdot i_{sf}^*; \end{cases} \quad \begin{cases} P_r = 2 \cdot V_{rf} \cdot i_{rf}; \\ Q_r = 2 \cdot V_{rf} \cdot i_{rf}^*; \end{cases} \tag{5}$$

$$i_{rf} = \frac{P_r}{2 \cdot V_{rf}}; \quad i_{rb} = i_{rf}^* = \frac{Q_r}{2 \cdot V_{rf}}, \tag{6}$$

where i_{rf}^* is the conjugate of i_{rb}.

This transformation enables the decoupling of system dynamics, simplifying the independent control of power components in each reference frame. Consequently, the torque is expressed as:

$$T_e = 2 \cdot p \cdot M \cdot \left[i_{sf} \cdot i_{rf}^* \right]. \tag{7}$$

Advanced SMC strategy for DFIGs. SMC is a nonlinear control methodology renowned for its robustness against uncertainties and external disturbances. The technique involves driving the system state toward a predefined sliding surface and maintaining it on this surface to achieve desired performance metrics. In the context of a DFIG, the control objective is to regulate rotor currents to ensure the generator delivers the specified active power while maintaining operational stability. A sliding surface is designed based on the error between the measured and reference rotor currents. Additionally, the SMC approach offers a rapid dynamic response, making it particularly suitable for systems requiring swift and precise adjustments. The control scheme's simplicity and computational efficiency contribute to its practical implementation in real-time systems, where high performance and minimal computational load are essential. The sliding surface can be defined as:

$$S_i = x_i^{ref} - x_i . \tag{8}$$

The sliding surface associated with each controlled (state) variable is x_i. Then, slide surface is presented by:

$$S_i = 0. \tag{9}$$

This formulation of the sliding surface ensures that ensuring that the dynamics of the controlled variables remain stable and the desired objectives are achieved with high precision. In the case of the reference x_i^{ref} is constant, the derivative of S_i in time-dependent is:

$$S_i = \frac{\mathrm{d}}{\mathrm{d}t}\left(x_i^{ref} - x_i \right) = -\frac{\mathrm{d}x_i}{\mathrm{d}t}. \tag{10}$$

Equation (10) can be rewritten as:

$$S_i = -\sum_{j=1}^{n} a_{ij} \cdot x_i - \sum_{k} b_k^1 \cdot u_k , \tag{11}$$

for a linear system of order n and in the absence of disturbances.

In the Ku framework, a single input u_i is directly associated with S_i, leading to the following relationship:

$$S_i = -\sum_{j=1}^{n} a_{ij} \cdot x_j - b_i \cdot u_i , \tag{12}$$

where u_i is defined as:

$$u_i = \frac{1}{b_i}\left(-S_i - \sum_{j=1}^{n} a_{ij} \cdot x_j \right), \tag{13}$$

where $\sum_{j=1}^{n} a_{ij} \cdot x_j$ is the term that corresponding to the control input required on the slide surface ($S_i = 0$) and S_i is the term which leads the regulated state variable towards the slide surface. To guarantee the stability we use the Lyapunov criterion that we apply to S_i:

$$S_i \cdot S_i < 0 . \tag{14}$$

Then we have:

$$S_i = -q \cdot \mathrm{sign}(S_i) - k \cdot S_i , \tag{15}$$

or

$$S_i = -k \left| S_i \right|^{\alpha} \cdot \mathrm{sign}(S_i) \quad \text{with} \quad 0 < \alpha < 1 , \tag{16}$$

where q is the positive (q>0) control gain related to the switching action; k is the positive (k>0) linear feedback gain that introduces a damping effect; α is the nonlinear exponent that modifies the surface dynamics, allowing finite-time convergence and further reduction of chattering effects.

A nonlinear sliding surface is defined as a function of the system's state variables, enabling the derivation of control inputs. The methodology involves designing an appropriate sliding surface and computing the equivalent nonlinear control values for each regulated variable. By leveraging the Ku transformation, the sliding surfaces for the rotor currents are formulated as follows:

$$\begin{cases} S(i_{rf}) = \left(i_{rf}^{ref} - i_{rf} \right); \\ S(i_{rb}) = S\left(i_{rf}^* \right). \end{cases} \tag{17}$$

The derived of the surfaces gives:

$$\begin{cases} S(i_{rf}) = \left(i_{rf}^{*ref} - i_{rf}^* \right); \\ S(i_{rb}) = \left(i_{rb}^{*ref} - i_{rb}^* \right). \end{cases} \tag{18}$$

After the calculation we have:

$$\begin{cases} S(i_{rf}) = \left(i_{rf}^{*ref} + \frac{1}{L_r} \cdot \left(V_{rf} - R_r \cdot i_{rf} + j \cdot \omega_r \cdot \varphi_{rf} \right) \right); \\ S(i_{rb}) = S\left(i_{rf}^* \right) \end{cases} \tag{19}$$

We put $V_{rf} = V_{rf}^{eq} + V_{rf}^{n}$ and $V_{rb} = V_{rb}^{eq} + V_{rb}^{n}$ then the control becomes:

$$\begin{cases} S(i_{rf}) = i_{rf}^{*ref} + \frac{1}{L_r} \cdot \left(\left(V_{rf}^{eq} + V_{rf}^{n} \right) - R_r \cdot i_{rf} + j \cdot \omega_r \cdot \varphi_{rf} \right); \\ S(i_{rb}) = S\left(i_{rf}^* \right) \end{cases} \tag{20}$$

In the steady state the sliding mode is:

$S_i = 0$, $S(i) = 0$, $V_{rf}^{n} = 0$ and $V_{rb}^{n} = 0$.

Then the rotor voltage expression becomes:

$$\begin{cases} V_{rf} = V_{rf}^{eq} + V_{rf}^{n}; \\ V_{rb} = V_{rf}^{*}. \end{cases} \tag{21}$$

Consequently, the commutation terms are:

$$\begin{cases} V_{rf}^{n} = k \cdot V_{rf} \cdot \mathrm{sign}\left(S(i_{rf}) \right); \\ V_{rb}^{n} = V_{rf}^{n*}. \end{cases} \tag{22}$$

Study of unbalanced voltage effects on DFIG operation.

1. Unbalanced supply voltage modelling. Modelling unbalanced supply voltage disturbances is essential to understanding their impact on systems like the DFIG. Voltage unbalance occurs when the three-phase voltages have unequal amplitudes or are not 120° out of phase, often due to phase loss, single-phase loads, or issues in

the power source. This unbalance can significantly reduce motor lifespan and lead to voltage drops, interrupting industrial processes. These transients, with varying amplitude and frequency, can degrade or destroy motor winding insulation. It is recommended to avoid operating motors with a voltage unbalance greater than 5 %, as this can cause a current unbalance of around 40 %. The calculation of unbalance can be approximated by the voltage unbalance factor (VUF, in %) equation that is the expression of the Standards [33–35]:

$$\text{VUF} = (V_n / V_p)\cdot 100\ \%,$$

where V_p, V_n are the amplitudes of the positive and negative sequence, respectively.

The unbalanced supply voltage can be expressed as:

$$V_{unb}(t) = V_{ref}\cdot(1+\delta(t)), \tag{23}$$

where V_{ref} is the reference voltage underbalanced conditions; $\delta(t)$ is the voltage deviation due to the imbalance, which varies over time.

The total unbalance in the system can be quantified using VUF, which measures the degree of unbalance, with higher values indicating greater imbalance:

$$VUF = \frac{\sqrt{(\Delta V_a)^2 + (\Delta V_b)^2 + (\Delta V_c)^2}}{V_{ref}}, \tag{24}$$

where ΔV_a, ΔV_b, ΔV_c are the deviations in each phase due to the unbalance.

Voltage unbalance is assumed at the stator, directly connected to the grid, eliminating the need to reconfigure the machine's equations. Since control is applied at the rotor level, it remains unaffected by the unbalance, requiring no adjustments. Under unbalanced conditions, only the stator's electrical equation is modified to account for unbalanced voltages, while the rotor's electrical and mechanical equations remain unchanged:

$$V_{sf} = \sqrt{\frac{3}{2}}\left(V_{sd}e^{+i\omega t} + V_{si}e^{-i\omega t}\right), \tag{25}$$

where V_{sd}, V_{si} are the RMS values of the direct and inverse sequence voltages, respectively; and:

$$\begin{cases} i_{sf} = i_{sfd} + i_{sfi}; \\ i_{sb} = i_{sf}^{*}. \end{cases} \tag{26}$$

Unbalanced supply voltage disturbances are a common issue in DFIGs used in wind energy systems. These disturbances can significantly impact system performance and stability, causing torque ripple, increased power losses, overheating of components, and a reduced system lifespan. Additionally, they impair the effectiveness of the voltage controller, leading to less efficient power generation.

2. Mathematical modelling of voltage imbalance impact on DFIG performance. To account for the voltage imbalance in the DFIG, the equations governing active and reactive power need to be adjusted.

Indeed, in the case of an unbalanced supply voltage, these equations must account for the voltage deviations ΔV_a, ΔV_b, ΔV_c, which will modify the power calculations and the control strategies used to maintain stability. After considering the unbalanced stator voltages $V_a^{'}$, $V_b^{'}$, $V_c^{'}$:

$$V_a^{'} = V_a + \Delta V_a;\quad V_b^{'} = V_b + \Delta V_b;\quad V_c^{'} = V_c + \Delta V_c. \tag{27}$$

The active power P and the reactive power Q provided by the DFIG are expressed as:

$$\begin{cases} P = \frac{3}{2}\left(V_a^{'}\cdot I_a^{*} + V_b^{'}\cdot I_b^{*} + V_c^{'}\cdot I_c^{*}\right), \\ Q = \frac{3}{2}\left(V_a^{'}\cdot I_a^{*'} + V_b^{'}\cdot I_b^{*'} + V_c^{'}\cdot I_c^{*'}\right), \end{cases} \tag{28}$$

where I_a^{*}, I_b^{*}, I_c^{*} are the complex conjugates of the currents in each phase; $I_a^{*'}$, $I_b^{*'}$, $I_c^{*'}$ are the phase currents in quadrature with the voltages.

The inclusion of ΔV_a, ΔV_b, ΔV_c, in the voltages leads to changes in the reactive power produced by the system. The electromagnetic torque T_{em} produced by the DFIG is directly related to the active power P and the rotor speed ω_r. Under balanced conditions, the torque can be expressed as:

$$T_{em} = P/\omega_r. \tag{29}$$

The revised equation for the electromagnetic torque, taking into account the voltage deviations, can be expressed as:

$$T_{em}^{'} = P^{'}/\omega_r. \tag{30}$$

Power losses P_{loss} in the system can increase due to unbalanced voltages, as they cause higher currents and additional losses in both the stator and rotor circuits:

$$P_{loss} = R_s\cdot I_s^2 + R_r\cdot I_r^2, \tag{31}$$

where R_s, R_r are the stator and rotor resistances; I_s, I_r are the currents in the stator and rotor under unbalanced voltage conditions. These currents increase due to the imbalance, leading to higher losses. As a result, the efficiency η is reduced due to the increased losses.

$$\eta = \frac{P_{out}}{P_{in}} = \frac{P_{out}}{P_{out} + P_l}, \tag{32}$$

where P_l is the mechanical output power; P_{in}, P_{out} are the electrical input and output powers. Under unbalanced voltage conditions, as losses increase, the efficiency decreases.

3. Active fault-tolerant control description. The primary goal of the AFT-SMC strategy is to maintain the operational performance of the DFIG by enabling rapid fault detection and adaptive control adjustments to mitigate their impact, thereby ensuring high equipment availability and system reliability. AFT-SMC is particularly well suited to this application because of its robustness to disturbances and its ability to react quickly and effectively to faults. This rapid response reduces service interruptions and improves the overall resilience of the system, even in degraded conditions.

AFT-SMC is a strategy designed to maintain safe and effective system operation despite faults, which is crucial for critical systems like DFIGs in wind turbines. AFT-SMC consists of 4 key components (Fig. 1): fault detection, fault isolation, reconfiguration, and system adaptation. The fault detection block identifies anomalies in the system and activates the reconfiguration mechanism quickly.

The fault isolation block minimizes the impact of the fault, typically through modularization. Finally, the reconfiguration mechanism adapts the controller to the system's behavior in both normal and faulty conditions. After detecting, locating, and identifying the fault, the system must adopt a strategy that ensures continued operation while providing accurate information about the faulty situation.

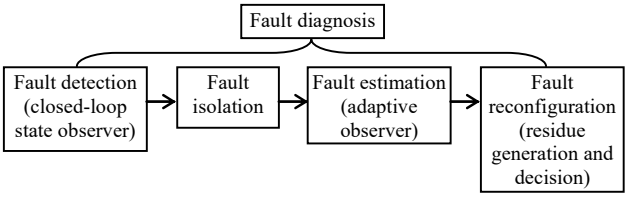

Fig. 1. AFT-SMC strategy scheme

Fault detection can be modelled using a criterion based on monitoring key system parameters. This approach involves tracking the deviation of parameter values from normal operating thresholds.

$$\delta(t) = \left| y(t) - y_{ref}(t) \right|, \tag{33}$$

where $y(t)$ is the system's output; $y_{ref}(t)$ is the reference value (the expected value). If $\delta(t)$ exceeds a critical threshold $\delta_{th}(t)$, a fault is detected. We have:

- fault detected if: $\delta(t) > \delta_{th}(t)$;
- no fault if: $\delta(t) \le \delta_{th}(t)$.

Fault isolation identifies the specific location of a fault within the system, aiming to minimize deviation errors by precisely isolating the fault's origin. A common localization technique uses the deviation of outputs from each component to identify the origin of the fault. For a DFIG, fault isolation can be represented by the deviation between observed system values and those predicted under various fault scenarios, enabling precise identification of the fault location.

$$e(t) = \hat{y}(t) - \tilde{y}(t), \tag{34}$$

where $\hat{y}(t)$, $\tilde{y}(t)$ are the estimated and actual system outputs. The error is defined as the difference between them.

When an abnormality is detected and isolated, the controller is reconfigured to adapt to the changed operating conditions. This adjustment involves updating the control model to mitigate the impact of the fault. The active and reactive power control equations are therefore modified as:

$$\begin{cases} P = V_s \cdot I_s \cdot \cos(\theta_s - \theta_r); \\ Q = V_s \cdot I_s \cdot \sin(\theta_s - \theta_r), \end{cases} \tag{35}$$

where θ_s, θ_r are the respective angles of the stator and rotor voltages.

Indeed, the control must be adjusted to compensate for the loss of performance as well as the change in the system's behavior. This should be done by modifying the converter or generator control:

$$\begin{cases} P_{re} = P + \Delta P; \\ Q_{re} = Q + \Delta Q, \end{cases} \tag{36}$$

where P_{re}, Q_{re} are the active and reactive reconfigured power; ΔP, ΔQ are the necessary adjustments to maintain the system's balance after the fault.

When a fault is identified, the controller must modify its behavior in response to the diagnostic information to effectively handle the changed conditions. This adaptive controller is represented by a dynamic gain function that adjusts according to the system parameters:

$$u(t) = K(t) \cdot e(t), \tag{37}$$

where $u(t)$ is the controller output (control signal); $K(t)$ is an adaptive gain that depends on the system's operating conditions and the detected errors; $e(t)$ is the error between the measured output and the reference output.

To mitigate the effects of voltage unbalance, the control system must dynamically adapt the operation of the generator and converter to maintain system stability and ensure efficient energy delivery. This is achieved through adjustments to the converter duty cycle, reconfiguration of control parameters, or compensation for the imbalance by modulating the generator output. Consequently, the stator active and reactive power equations are updated as:

$$\begin{cases} P_s = V_{sf} \cdot \left(i_{sfd} + i_{sfi}\right) + V_{sf}^* \cdot i_{sf}^*; \\ Q_s = V_{sf}^* \cdot \left(i_{sfd} + i_{sfi}\right) + V_{sf} \cdot i_{sf}^*. \end{cases} \tag{38}$$

In this transformation i_{sf} is the conjugate of i_{sb}. Then:

$$\begin{cases} P_s = 2 \cdot V_{sf} \cdot \left(i_{sfd} + i_{sfi}\right); \\ Q_s = 2 \cdot V_{sf}^* \cdot \left(i_{sfd} + i_{sfi}\right). \end{cases} \tag{39}$$

Simulation results and discussions.

1. Healthy condition. To demonstrate the effectiveness of the control approach, we use MATLAB. First, to confirm the effectiveness of the control, we represent the sliding surfaces (Fig. 2). We observe the fastest convergence time and the least amount of interference in the control.

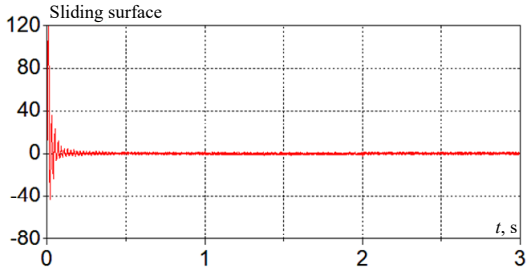

Fig. 2. Sliding surface in healthy situation

In Fig. 3, 4, the active and reactive powers in the output sliding mode control perfectly follow the desired variables. We note that the outputs are fast during the transient state, and the static error tends to zero. The results indicate that the control dynamics exhibit rapid response and accurately track the steady-state reference with negligible static error.

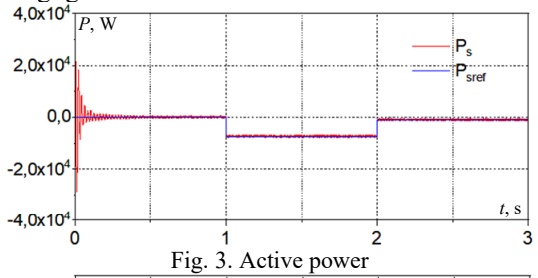

Fig. 3. Active power

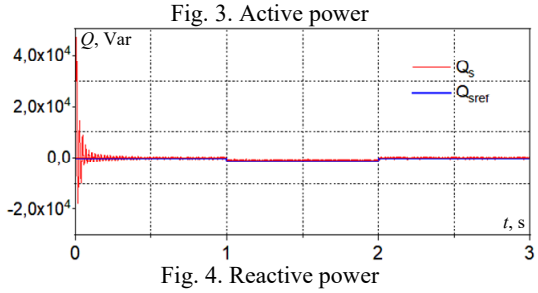

Fig. 4. Reactive power

Figure 5 shows the stator fluxes curves, where the flux-oriented strategy is clearly observable. Figure 6 provides a detailed presentation of the generated stator

voltage (phase A) and its associated current. We notice that the generated stator voltage meets the desired amplitude and frequency. From these results, we can conclude that speed regulation by sliding mode is satisfactory.

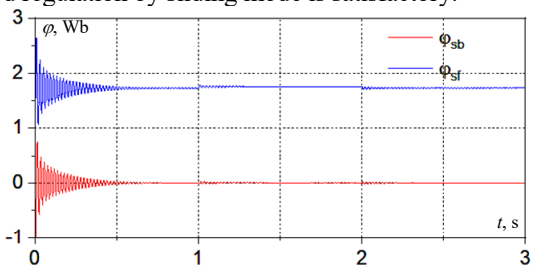

Fig. 5. Stator fluxes

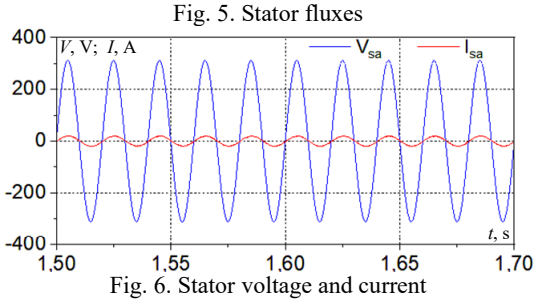

Fig. 6. Stator voltage and current

2. Faulty condition. An unbalanced fault occurs in one phase of the machine's stator supply.

In Fig. 7 we observe the effect of the fault on the sliding surface. We note that the sliding surface of the machine with the fault is significantly larger compared to the sliding surface without the fault.

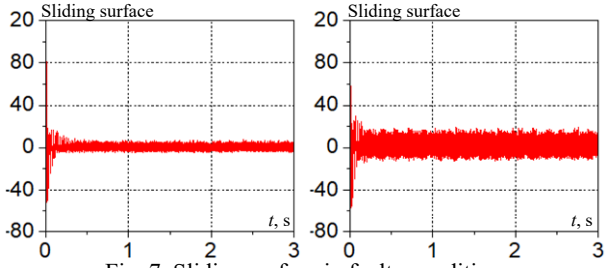

Fig. 7. Sliding surface in faulty condition

Indeed, unbalanced supply voltages can cause the DFIG to deviate from the desired sliding surface due to inaccuracies in the estimation of rotor currents or a mismatch between actual and reference values.

We also observe excessive oscillations when the fault occurs. These oscillations vary within a maximum interval, a phenomenon known as chattering. Despite these oscillations, the control remains accurate to its set-point. Therefore, the control design is clearly independent of the disturbance applied to the system.

The fault-tolerant control performance of the DFIG is demonstrated in Fig. 8–10 under 30 % voltage unbalance. The strategy exhibits robustness, as evidenced by the consistent tracking of the reference set-point despite oscillations around the target value. To implement an adaptive fault-tolerant control scheme, residual signatures from the control parameters must be defined and analyzed. The key goal of fault-tolerant control is to identify and interpret fault-induced spectral characteristics within the system, enabling effective mitigation and adaptive system response. Indeed, to extract the specific fault signatures and highlight our results, a spectral analysis of the active power is conducted. The chosen diagnostic method is based on fast Fourier transform (FFT).

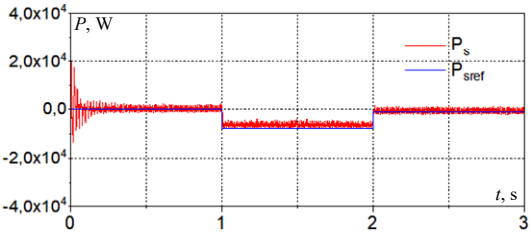

Fig. 8. Active power after unbalanced supply voltage condition

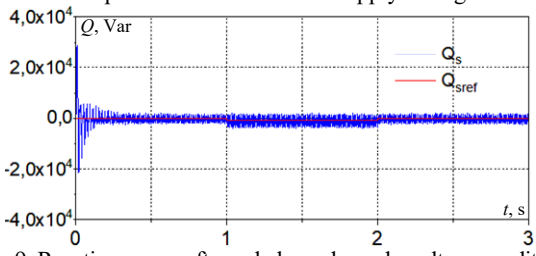

Fig. 9. Reactive power after unbalanced supply voltage condition

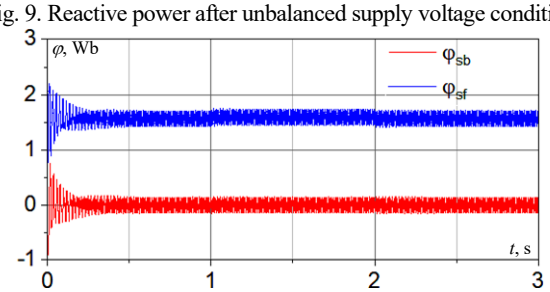

Fig. 10. Stator fluxes after unbalanced supply voltage condition

This model-based diagnostic approach involves detecting faults by studying certain frequency components that appear in the stator current and instantaneous stator power spectrums. The analysis of the spectral content of partial instantaneous power (the instantaneous power of a stator phase), as defined as the product of the line current, offers important insights for characterizing the voltage imbalance phenomenon in the machine.

Figure 11 shows the spectral characteristics of active power under voltage imbalance conditions.

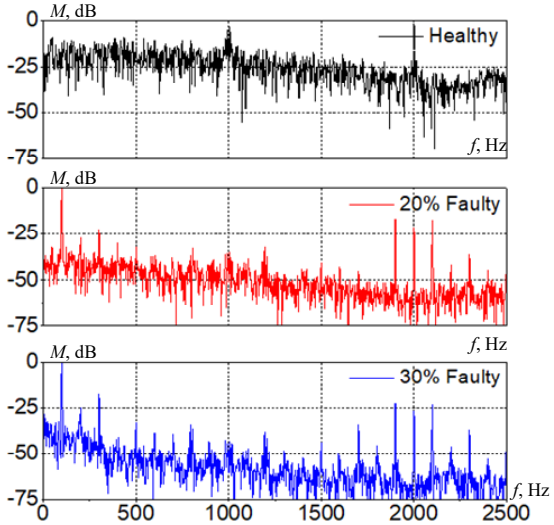

Fig. 11. Normalized spectrum of active power *P* under different conditions of voltage unbalance

Several frequency components may appear in the spectrum. The analysis reveals the existence of harmonic components at integer multiples of the fundamental frequency ($k \cdot f_s$), arising due to disturbances within the system. In the presence of voltage imbalance, the amplitude

of the harmonics varies from phase to phase, leading to an asymmetrical harmonic content in the active power spectrum. Imbalance frequencies become clearly noticeable when different levels of fault are applied. Their severity is linked to the increase in fault severity applied to the system.

Figure 12 shows the spectral content of the stator current I_{sa} under unbalanced supply voltage conditions. Voltage imbalance refers to the uneven distribution or asymmetry of voltage levels between the machine's phases. The frequency components examined in the stator current signal show an increase in certain harmonics directly related to the fault, as well as the appearance of other frequencies that are multiples of the fundamental. These frequencies cause multiple impacts of voltage imbalance on machine performance, including torque ripple, increased losses, and potential damage to the machine.

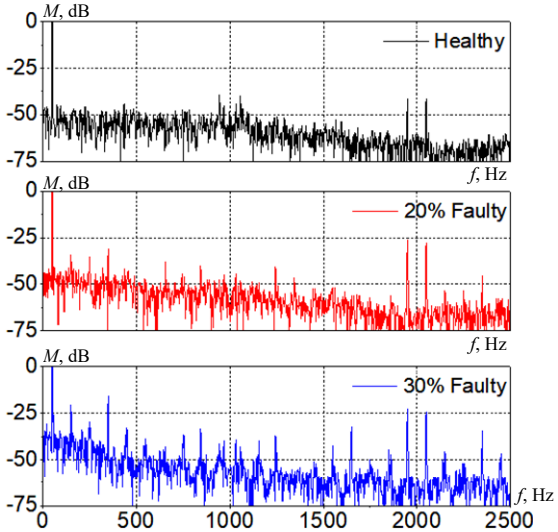

Fig. 12. Normalized spectrum of stator current I_{sa} under different conditions of voltage unbalance

Conclusions. This work introduces a robust active fault-tolerant strategy based on sliding mode control (AFT-SMC) for doubly-fed induction generators (DFIGs), combined with an advanced real-time spectral fault diagnosis system. The methodology addresses 2 major challenges in wind energy systems: maintaining system stability under severe grid disturbances, and accurately diagnosing electrical faults in real time.

Unlike conventional vector control schemes, the proposed AFT-SMC approach effectively mitigates the adverse effects of voltage unbalance, such as torque ripple and unstable current profiles, by dynamically adjusting the control surface based on fault severity. This is made possible by integrating a diagnostic module based on fast Fourier transform, which detects characteristic harmonic distortions in both the stator current and active power signals. These harmonic components are shown to correlate directly with fault magnitude, enabling a precise and adaptive fault response mechanism.

Extensive simulation results conducted under a realistic 30 % voltage unbalance scenario demonstrate the superior performance of the proposed strategy. The controller achieves a voltage recovery time of approximately 0.28 s, compared to 0.42 s with standard vector control, highlighting faster system stabilization. Moreover, electromagnetic torque oscillations are reduced by around 45 %, significantly lowering mechanical stress and enhancing system lifespan. The integrated diagnostic system further achieves a fault classification accuracy of 94.6 %, ensuring early fault identification and improving operational reliability. These quantitative results confirm that the proposed AFT-SMC framework not only improves transient and steady-state performance but also advances fault resilience through embedded intelligence. By integrating control and diagnosis within a unified framework, the proposed methodology offers a powerful solution for predictive maintenance, minimizing downtime and significantly improving the operational reliability of wind turbine systems. This work establishes a solid foundation for future deployment in large-scale renewable energy infrastructures, where resilience to faults, autonomous operation, and efficiency are paramount. Although the current validation is based on detailed and realistic simulations, future research will focus on experimental implementation to assess the controller's performance under real-world conditions.

This progressive research pathway, from rigorous simulation to practical validation, reinforces the robustness, scalability, and technological relevance of the proposed strategy. In summary, the developed AFT-SMC approach represents a significant and practical advancement in fault-tolerant control of DFIG-based wind energy systems. It addresses key challenges in modern smart grids and holds strong promise for accelerating the integration of reliable, intelligent renewable energy technologies on a large scale.

Conflict of interest. The authors declare that they have no conflicts of interest.

REFERENCES

1. Qazi A., Hussain F., Rahim N.A., Hardaker G., Alghazzawi D., Shaban K., Haruna K. Towards sustainable energy: a systematic review of renewable energy sources, technologies, and public opinions. *IEEE Access*, 2019, vol. 7, pp. 63837-63851. doi: https://doi.org/10.1109/ACCESS.2019.2906402.

2. Ahmed M., Shimada K. The effect of renewable energy consumption on sustainable economic development: evidence from emerging and developing economies. *Energies*, 2019, vol. 12, no. 15, art. no. 2954. doi: https://doi.org/10.3390/en12152954.

3. Sun L., Mi Z., Yu Y., Wu T., Tian H. Active power and reactive power regulation capacity study of DFIG wind turbine. *2009 International Conference on Sustainable Power Generation and Supply*, 2009, pp. 1-6. doi: https://doi.org/10.1109/SUPERGEN.2009.5348144.

4. Ghennam T., Berkouk E.M., Francois B. Modeling and control of a Doubly Fed Induction Generator (DFIG) based Wind Conversion System. *2009 International Conference on Power Engineering, Energy and Electrical Drives*, 2009, pp. 507-512. doi: https://doi.org/10.1109/POWERENG.2009.4915230.

5. Kaddache M., Drid S., Khemis A., Rahem D., Chrifi-Alaoui L. Maximum power point tracking improvement using type-2 fuzzy controller for wind system based on the double fed induction generator. *Electrical Engineering & Electromechanics*, 2024, no. 2, pp. 61-66. doi: https://doi.org/10.20998/2074-272X.2024.2.09.

6. Bouraghda S., Sebaa K., Bechouat M., Sedraoui M. An improved sliding mode control for reduction of harmonic currents in grid system connected with a wind turbine equipped by a doubly-fed induction generator. *Electrical Engineering & Electromechanics*, 2022, no. 2, pp. 47-55. doi: https://doi.org/10.20998/2074-272X.2022.2.08.

7. Kini P.G., Bansal R.C., Aithal R.S. A novel approach toward interpretation and application of voltage unbalance factor. *IEEE Transactions on Industrial Electronics*, 2007, vol. 54, no. 4, pp. 2315-2322. doi: https://doi.org/10.1109/TIE.2007.899935.

8. Jannati M., Idris N.R.N., Salam Z. A new method for modeling and vector control of unbalanced induction motors. *2012 IEEE Energy*

Conversion Congress and Exposition (ECCE), 2012, pp. 3625-3632. doi: https://doi.org/10.1109/ECCE.2012.6342483.
9. Touil A., Babaa F. Studying of unbalanced supply voltage effects on three-phase induction motor performances based on line neutral voltage analytical calculation. *Lecture Notes in Electrical Engineering*, 2024, vol. 1147 LNEE, pp. 455-467. doi: https://doi.org/10.1007/978-981-97-0045-5_41.
10. Maurer F., Toftevaag T.L., Noland J.K. An analytical prediction model of balanced and unbalanced faults in doubly fed induction machines. *IEEE Transactions on Industrial Electronics*, 2023, vol. 70, no. 1, pp. 189-199. doi: https://doi.org/10.1109/TIE.2022.3146540.
11. Barambones O., Alkorta P. Position control of the induction motor using an adaptive sliding-mode controller and observers. *IEEE Transactions on Industrial Electronics*, 2014, vol. 61, no. 12, pp. 6556-6565. doi: https://doi.org/10.1109/TIE.2014.2316239.
12. Bennassar A., Banerjee S., Jamma M., Essalmi A., Akherraz M. Real time high performance of sliding mode controlled induction motor drives. *Procedia Computer Science*, 2018, vol. 132, pp. 971-982. doi: https://doi.org/10.1016/j.procs.2018.05.113.
13. Farhi S.E., Sakri D., Golea N. High-performance induction motor drive based on adaptive super-twisting sliding mode control approach. *Archives of Electrical Engineering*, 2022, vol. 71, no. 1, pp. 245-263. doi: https://doi.org/10.24425/aee.2022.140208.
14. Fetene Y., Shibeshi D. Fractional order sliding mode speed control of feedback linearized induction motor. *Power Electronics and Drives*, 2020, vol. 5, no. 1, pp. 109-122. doi: https://doi.org/10.2478/pead-2020-0010.
15. Lascu C., Argeseanu A., Blaabjerg F. Supertwisting sliding-mode direct torque and flux control of induction machine drives. *IEEE Transactions on Power Electronics*, 2020, vol. 35, no. 5, pp. 5057-5065. doi: https://doi.org/10.1109/TPEL.2019.2944124.
16. Jafarian M.J., Nazarzadeh J. Spectral analysis for diagnosis of bearing defects in induction machine drives. *IET Electric Power Applications*, 2019, vol. 13, no. 3, pp. 340-348. doi: https://doi.org/10.1049/iet-epa.2018.5226.
17. Boudali A., Negadi K., Boudiaf M., Berkani A., Marignetti F. Super twisting sliding mode controller of small hydropower plant energy generation based DFIG. *Przegląd Elektrotechniczny*, 2020, vol. 96, no. 10, pp. 136-143. doi: https://doi.org/10.15199/48.2020.10.25.
18. Begam S.R., Burthi L.R., Depuru S.R. Adaptive neuro-fuzzy sliding mode controller (ANF-SMC) to control speed, electromagnetic torque (EMT), stator current, and back EMF using PMBLDCmotor(PMBLDCM) in electric propulsion of electric vehicles. *Przegląd Elektrotechniczny*, 2023, no. 8, pp. 49-62. doi: https://doi.org/10.15199/48.2023.08.09.
19. Sakri D., Laib H., Farhi S.E., Golea N. Sliding mode approach for control and observation of a three phase AC-DC pulse-width modulation rectifier. *Electrical Engineering & Electromechanics*, 2023, no. 2, pp. 49-56. doi: https://doi.org/10.20998/2074-272X.2023.2.08.
20. Wang X., Wang Z., Xu Z., He J., Zhao W. Diagnosis and tolerance of common electrical faults in T-type three-level inverters fed dual three-phase PMSM drives. *IEEE Transactions on Power Electronics*, 2020, vol. 35, no. 2, pp. 1753-1769. doi: https://doi.org/10.1109/TPEL.2019.2920400.
21. Bolognani S., Zordan M., Zigliotto M. Experimental fault-tolerant control of a PMSM drive. *IEEE Transactions on Industrial Electronics*, 2000, vol. 47, no. 5, pp. 1134-1141. doi: https://doi.org/10.1109/41.873223.
22. Siddiqui K.M., Sahay K., Giri V.K. Stator Inter-turn fault detection in inverter fed induction motor drives. *International Journal of Applied Power Engineering (IJAPE)*, 2017, vol. 6, no. 2, pp. 89-102. doi: https://doi.org/10.11591/ijape.v6.i2.pp89-102.
23. Namdar A., Samet H., Allahbakhshi M., Tajdinian M., Ghanbari T. A robust stator inter-turn fault detection in induction motor utilizing Kalman filter-based algorithm. *Measurement*, 2022, vol. 187, art. no. 110181. doi: https://doi.org/10.1016/j.measurement.2021.110181.
24. Nikpayam M., Ghanbari M., Esmaeli A., Jannati M. Vector control methods for star-connected three-phase induction motor drives under the open-phase failure. *Journal of Operation and Automation in Power Engineering*, 2022, vol. 10, no. 2, pp. 155-164. doi: https://doi.org/10.22098/joape.2022.8802.1616.
25. Merabet A., Eshaft H., Tanvir A.A. Power-current controller based sliding mode control for DFIG-wind energy conversion system. *IET Renewable Power Generation*, 2018, vol. 12, no. 10, pp. 1155-1163. doi: https://doi.org/10.1049/iet-rpg.2017.0313.
26. Chavhan R., Kulkarni V.A. Negative sequence component for detection of inter-turn fault of transformer. *International Journal of Innovative Research in Science, Engineering and Technology*, 2017, vol. 6, no. 7, pp. 13950-13958. doi: https://doi.org/10.15680/IJIRSET.2017.0607172.
27. Huang G., Luo Y.-P., Zhang C.-F., Huang Y.-S., Zhao K.-H. Current sensor fault diagnosis based on a sliding mode observer for PMSM driven systems. *Sensors*, 2015, vol. 15, no. 5, pp. 11027-11049. doi: https://doi.org/10.3390/s150511027.
28. Jiang J., Yu X. Fault-tolerant control systems: a comparative study between active and passive approaches. *Annual Reviews in Control*, 2012, vol. 36, no. 1, pp. 60-72. doi: https://doi.org/10.1016/j.arcontrol.2012.03.005.
29. Amin A.A., Hasan K.M. A review of fault tolerant control systems: advancements and applications. *Measurement*, 2019, vol. 143, pp. 58-68. doi: https://doi.org/10.1016/j.measurement.2019.04.083.
30. Moussaoui L., Aouaouda S., Rouaibia R. Fault tolerant control of a permanent magnet synchronous machine using multiple constraints Takagi-Sugeno approach. *Electrical Engineering & Electromechanics*, 2022, no. 6, pp. 22-27. doi: https://doi.org/10.20998/2074-272X.2022.6.04.
31. Noura H., Sauter D., Hamelin F., Theilliol D. Fault-tolerant control in dynamic systems: application to a winding machine. *IEEE Control Systems Magazine*, 2000, vol. 20, no. 1, pp. 33-49. doi: https://doi.org/10.1109/37.823226.
32. Rahali H., Zeghlache S., Cherif B.D.E., Benyettou L., Djerioui A. Robust adaptive fuzzy type-2 fast terminal sliding mode control of robot manipulators in attendance of actuator faults and payload variation. *Electrical Engineering & Electromechanics*, 2025, no. 1, pp. 31-38. doi: https://doi.org/10.20998/2074-272X.2025.1.05.
33. *IEEE Recommended Practice for Monitoring Electric Power Quality. IEEE Std 1159-2009*, 26 June 2009, 94 p. doi: https://doi.org/10.1109/IEEESTD.2009.5154067.
34. *IEC 61000-4-30:2015+AMD1:2021 CSV. Electromagnetic compatibility (EMC) – Part 4-30: Testing and measurement techniques – Power quality measurement methods*, 2021, 292 p.
35. *Standard NRS 048-2:2003. Electricity Supply – Quality of Supply. Part 2: Voltage Characteristics, Compatibility Levels, Limits and Assessment Methods*. Standards South Africa, 2013. 33 p.

Received 07.06.2025
Accepted 13.08.2025
Published 02.11.2025

N. Hamdi [1], *Doctor of Electrical Engineering,*
F. Babaa [2], *Doctor of Electrical Engineering,*
A. Touil [2], *Doctor of Electrical Engineering,*
N. Merabet [2], *PhD,*
[1] Laboratory of Electronics and New Technology,
University of Oum El Bouaghi, Algeria,
e-mail: hamdi_naouel@yahoo.fr
[2] Electrical Laboratory of Constantine «LE »,
University Freres Mentouri Constantine 1, Algeria,
e-mail: babaa.fatima@yahoo.fr;
abderrahim.touil@lec-umc.org (Corresponding Author);
nacer.merabet1@doc.umc.edu.dz

How to cite this article:
Hamdi N., Babaa F., Touil A., Merabet N. Robust fault-tolerant sliding mode control and advanced fault diagnosis for doubly-fed induction generators. *Electrical Engineering & Electromechanics*, 2025, no. 6, pp. 32-39. doi: https://doi.org/10.20998/2074-272X.2025.6.05